Journal of Structural Biology 169 (2010) 116–123

Contents lists available at ScienceDirect

Journal of Structural Biology

journal homepage: www.elsevier.com/locate/yjsbi

Influence of the $g-$ conformation of Ser and Thr on the structure of transmembrane helices

Xavier Deupi [a,2], Mireia Olivella [b,2], Arantxa Sanz [a], Nicole Dölker [a,1], Mercedes Campillo [a], Leonardo Pardo [a,*]

[a] Laboratori de Medicina Computacional, Unitat de Bioestadística, Facultat de Medicina, Universitat Autònoma de Barcelona, 08193 Bellaterra, Spain
[b] Grup de Recerca en Bioinformàtica i Estadística Mèdica, Departament de Biologia de Sistemes, Escola Politècnica Superior, Universitat de Vic, 08500 Vic, Barcelona, Spain

ARTICLE INFO

Article history:
Received 7 May 2009
Received in revised form 8 September 2009
Accepted 15 September 2009
Available online 17 September 2009

Keywords:
Membrane proteins
Transmembrane helices
Serine/threonine
Helix kinks
Molecular dynamics

ABSTRACT

In order to study the influence of Ser and Thr on the structure of transmembrane helices we have analyzed a database of helix stretches extracted from crystal structures of membrane proteins and an ensemble of model helices generated by molecular dynamics simulations. Both complementary analyses show that Ser and Thr in the $g-$ conformation induce and/or stabilize a structural distortion in the helix backbone. Using quantum mechanical calculations, we have attributed this effect to the electrostatic repulsion between the side chain Oγ atom of Ser and Thr and the backbone carbonyl oxygen at position $i-3$. In order to minimize the repulsive force between these negatively charged oxygens, there is a modest increase of the helix bend angle as well as a local opening of the helix turn preceding Ser/Thr. This small distortion can be amplified through the helix, resulting in a significant displacement of the residues located at the other side of the helix. The crystal structures of aquaporin Z and the β_2-adrenergic receptor are used to illustrate these effects. Ser/Thr-induced structural distortions can be implicated in processes as diverse as ligand recognition, protein function and protein folding.

1. Introduction

While roughly 15–30% of the eukaryote genes encode membrane proteins (Fleishman et al., 2006), less than 2% of the structures deposited at the Protein Data Bank correspond to this class (http://pdbtm.enzim.hu/) (Tusnady et al., 2005). Transmembrane (TM) α-helical proteins constitute the majority of integral membrane proteins (Fleishman et al., 2006). In addition to canonical α-helices, these TM bundles are also formed by non-canonical π-like helices, 3_{10}-like helices and kinked helices (Rigoutsos et al., 2003). Predicting and quantifying distortions within TM segments is important for understanding processes as diverse as ligand recognition, protein function, and protein folding (Deupi et al., 2007; Bowie, 2005). Helix distortions are most commonly induced by Pro, which can be identified with more than 90% reliability simply by looking at Pro abundance in a multiple sequence alignment (Yohannan et al., 2004). However, it has been shown that other residues are also able to induce distortions in the structure of TMs (Rigoutsos et al., 2003). For instance, we have previously shown that both Ser and Thr residues, either alone (Ballesteros et al., 2000) or in combination with Pro (Govaerts et al., 2001; Deupi et al., 2004), also induce distinctive distortions in TMs. Membrane proteins, thus, incorporate in the sequence of their TMs specific residues like Pro, Gly, Ser, and Thr (Senes et al., 2000), introducing a flexible point and assisting in helix movements (Sansom et al., 2000) or stabilizing local regions of structural relevance.

In addition to its role in modulating the structure of TMs, Ser and Thr residues are also reported to play key roles in preserving the overall structure of membrane proteins (Lopez-Rodriguez et al., 2002), stabilizing the interactions between TMs (Dawson et al., 2002; Eilers et al., 2002), and regulating protein function (Munshi et al., 2003; Jongejan et al., 2005; Pellissier et al., 2009). In addition, mutations involving polar residues in TM segments are often associated with protein malfunction (Partridge et al., 2004; Smit et al., 2007), being the most common disease-causing mutations in membrane proteins (Joh et al., 2008).

These roles of Ser and Thr are ultimately encoded in the chemical properties of their polar side chains. The short side chains of Ser and Thr have a limited rotamer conformational space. The *gauche−* ($g-$), *gauche+* ($g+$), and *trans* (t) staggered conformations are strongly preferred relative to the eclipsed conformations. The only exception is the t conformation of Thr, which is unfavorable due to the steric clash of the side chain methyl group with the backbone carbonyl at the $i-3$ position (McGregor et al., 1987). Ser and Thr in $g+$ or $g-$ are capable to hydrogen bond the backbone carbonyl in the previous turn of the helix (McGregor et al., 1987).

* Corresponding author. Fax: +34 93 581 2344.
E-mail address: Leonardo.Pardo@uab.es (L. Pardo).
[1] Present address: Department of Theoretical and Computational Biophysics, Max Planck Institute for Biophysical Chemistry, Am Faßberg 11, 37077 Göttingen, Germany.
[2] These authors contributed equally to this work.

1047-8477/$ - see front matter © 2009 Elsevier Inc. All rights reserved.
doi:10.1016/j.jsb.2009.09.009

We have previously shown that the $g-$ conformation of Ser and Thr residues modifies the conformation of Ser/Thr-containing α-helices (Ballesteros et al., 2000). This conclusion was achieved from statistical analysis of crystal structures of mostly soluble proteins, with only four structures of membrane proteins included in the analysis. It has been suggested that the membrane environment considerably perturbs the rotamer frequencies compared to soluble proteins (Chamberlain and Bowie, 2004). Thus, the present study aims to provide additional insight into the structural consequences of the different rotamer conformations of Ser and Thr on the overall geometry of TMs, combining two complementary sets of structural data: a database of helix stretches extracted exclusively from crystal structures of membrane proteins, and ensembles of model TMs generated by molecular dynamics (MD) simulations in an explicit hydrophobic environment.

2. Methods

2.1. Database of transmembrane helix segments

The atomic coordinates of the membrane proteins listed in Table 1 were extracted from the RCSB Protein Data Bank (Berman et al., 2000). The coordinates of all TM stretches with a length of 12 residues and bearing Ala (as a control), Ser or Thr in the 8th position were extracted for analysis. Selection of longer stretches would have lead to a reduction of the sample size. Only stretches with Ala/Ser/Thr exposed to the membrane were kept for analysis, in order to avoid interfering effects from residues of the protein core. Membrane exposed residues were selected if the accessible surface of residues at position i (containing Ala/Ser/Thr) and at position $i-4$ in the protein was larger than 60 Å^2 as calculated with the Naccess program (Hubbart and Thornton, 1993). Stretches with Pro residues in the sequence were removed from the database, to leave out Pro-induced structural distortions. The side chain conformation of Ser and Thr was categorized according to the value of its χ_1 dihedral angle into $g-$ (0–120°), t (120–240°), or $g+$ (240–360°), resulting in seven groups of TM segments: Ser$^{PDB}g-$, Ser$^{PDB}g+$, Ser^{PDB}t, Thr$^{PDB}g-$, Thr$^{PDB}g+$, Thr^{PDB}t, and Ala^{PDB}.

2.2. Molecular dynamics simulations

In order to generate a theoretical structural ensemble of TMs we performed unrestrained MD simulations on the helical model peptides Ace-(Ala)$_{11}$-X-(Ala)$_{12}$-NHMe, where X is either Ala (control), or Ser/Thr built in the $\chi_1 = g+$ and $g-$ rotamer conformations (Ala^{MD}, Ser$^{MD}g+$, Ser$^{MD}g-$, Thr$^{MD}g+$, Thr$^{MD}g-$). In contrast to Thr in $g-$, whose methyl group prevents the hydrogen bond interaction with the carbonyl oxygen at position $i-3$ (Deupi et al., 2004), Ser in $g-$ can hydrogen bond either the backbone carbonyl at position $i-3$ or at position $i-4$ (Ballesteros et al., 2000). Thus, we performed two additional restrained MD simulations of Ser in $g-$ with its Hγ atom hydrogen bonding the $i-3$ (OγH$\cdots$O$_{i-3}$) or $i-4$ (OγH$\cdots$O$_{i-4}$) carbonyls in the previous turn of the helix (Ser$^{MD}i-3$, Ser$^{MD}i-4$). The initial structures were placed in a rectangular box (approximately 62 Å × 55 Å × 55 Å) of methane molecules to mimic the hydrophobic environment. We have shown that this procedure reproduces the structural characteristics of TMs (Olivella et al., 2002). After equilibration of the solvent molecules, the entire system was subjected to 500 iterations of energy minimization and heated (from 0 to 300 K in 15 ps). This was followed by an equilibration period (15–500 ps) and a production run (500–1500 ps). Trajectories for such small model systems (<300 atoms) have converged after the equilibration period (0.5 ns). The statistical tests used to compare the structural features can only be applied to independent samples (see below). To

Table 1
Protein Data Bank identification code (PDB ID), protein name and X-ray resolution of membrane proteins used in the manuscript. These proteins are classified in superfamilies according to the OPM database (http://opm.phar.umich.edu/) (Lomize et al., 2006).

PDB ID	Protein name	Resolution (Å)
1.1.01. Rhodopsin-like proteins		
1c3w	Bacteriorhodopsin	1.55
1e12	Halorhodopsin	1.8
1h2s	Sensory rhodopsin	1.93
1uaz	Archaerhodopsin-1	3.4
1vgo	Archaerhodopsin-2	2.5
1l9 h	Rhodopsin	2.6
1.1.02. Photosynthetic reaction centers and photosystems		
1prc	*Rhodopseudomonas viridis* photosynthetic reaction center	2.35
1eys	*Thermochromatium trepidum* photosynthetic reaction center	2.2
1ogv	*Rhodobacter sphaeroides* light harvesting complex	2.35
	Thermosynechococcus elongatus photosystem II	3.0
1izl	*Thermocynechococcus vulcanus* photosystem II	3.7
1.1.03. Light-harvesting complexes		
1rwt	*Spinacia oleracea* light harvesting complex	2.72
1nkz	*Rhodopseudomonas acidophila* light harvesting complex	2.0
1lgh	*Rhodospirillum molischianum* light harvesting complex	2.4
1.1.04. Transmembrane cytochrome b like		
1vf5	*Mastigocladus laminosus* cytochrome b6f complex	3.0
1q90	*Chlamydomonas reinhardtii* cytochrome b6f complex	3.1
1qla	Fumarate reductase	2.2
1kqg	Formate dehydrogenase-N	2.8
1bcc	Chicken cytochrome bc1 complex	3.16
1bgy	Bovine cytochrome bc1 complex	3.0
1ezv	Yeast cytochrome bc1complex	2.3
1nek	Succinate dehydrogenase	2.6
1zoy	Succinate ubiquinone oxidoreductase	2.4
1q16	NarGHI nitrate reductase A	1.9
1.1.05. Cytochrome c oxidases		
1occ	aa3 cytochrome *c* oxidase	2.8
1ehk	ba3 cytochrome *c* oxidase	2.4
2gsm	Two-subunit catalytic core of cytochrome *c* oxidase	2.0
1fft	bo3 cytochrome ubiquinol oxidase	3.5
1.1.06. Proton or sodium translocating F-type, V-type and A-type ATPases		
2bl2	Rotor of V-type Na^+-ATPase	2.1
1yce	Rotor of F-type Na^+-ATPase	2.4
1.1.07. Methane monooxygenase		
1yew	Particulate methane monooxygenase	2.8
1.1.08. P-type ATPase (P-ATPase)		
1su4	Calcium P-type ATPase transporter	2.6
1.1.09. Vitamin B12 transporter-like ABC transporters		
1l7v	BtuCD vitamin B12 transporter	3.2
2nq2	HI1470/1 putative metal-chelate-type ABC transporter	2.4
1.1.10. Lipid flippase-like ABC transporters		
2hyd	Sav1866 multidrug transporter	3.0
1.1.12. General secretory pathway (Sec)		
1rhz	SecYEB protein-conducting channel	3.5
1.1.14. Major facilitator superfamily (MFS)		
1pv7	LacY lactose permease Transporter	3.5
1pw4	GlpT glycerol-3-phosphate transporter	3.3
2gfp	EmrD multidrug transporter	3.5
1.1.15. Resistance-nodulation-cell division		
2gif	AcrB bacterial multidrug efflux transporter	2.9
1.1.16. Dicarboxylate/amino acid:cation symporter (DAACS)		
1xfh	Glutamate transporter homolog	3.5
1.1.17. Monovalent cation/proton antiporter (CPA)		
1zcd	NhaA Na^+/H^+ antiporter	3.45
1.1.18. Ligand/cation symporters		
2a65	LeuTAa leucine transporter	1.65
1.1.19. Ammonia transporter (Amt)		
1xqf	AmtB ammonia channel	1.8

(*continued on next page*)

Table 1 (*continued*)

PDB ID	Protein name	Resolution (Å)
2b2f	Amt-1 ammonium transporter	1.54
1.1.22. Voltage-gated channel like		
1k4c	KcsA potassium channel H^+ gated	2.0
1orq	KvAP voltage-gated potassium channel	3.2
1ors	KvAP voltage-gated potassium channel	1.9
2a79	Kv1.2 voltage-gated potassium channel	2.9
1xl4	KirBac3.1 inward-rectifier potassium channel	2.6
2ahy	NaK channel	2.4
1lnq	MthK potassium channel, Ca^{2+} gated	3.3
1msl	MscL mechanosensitive channel	3.5
1.1.24. Small conductance mechanosensitive ion channel (MscS)		
2oau	MscS voltage-modulated mechanosensitive channel	3.7
1.1.27. Major intrinsic protein (MIP)		
1j4n	AQP1 aquaporin water channel	2.2
2f2b	AQPM aquaporin water channel	1.68
1rc2	AQPZ aquaporin water channel	2.5
1z98	SoPIP2 plant aquaporin	2.1
1fx8	GlpF glycerol facilitator channel	2.2
1.1.28. Chloride channel (ClC)		
1kpl	ClC chloride channel	3.5
1.1.32. Outer membrane auxiliary proteins		
2j58	Wza translocon for capsular polysaccharides	2.25
1.1.33. Disulfide bond oxidoreductase-B (DsbB)		
2hi7	DsbB–DsbA periplasmic oxidase complex	3.7
1.1.34. Multi-heme cytochromes		

achieve this prerequisite, structures were collected for analysis every 10 ps during the production run (1 ns), so that a given structure is not related to the previous and following structures (Lyapunov instability) (Frenkel and Smit, 1996), thus obtaining a structural ensemble of 100 structures for each model system. Simulations were carried out at constant volume and temperature (300 K), with the latter maintained through coupling to a heat bath. The particle mesh Ewald method was employed to compute electrostatic interactions. The MD simulations were run with the Sander module of AMBER 9 (Case et al., 2006), using the ff99SB force field (Hornak et al., 2006), SHAKE bond constraints on all bonds and a 2 fs integration time step.

The molecular mechanics/Poisson–Boltzmann solvent-accessible method (MM-PBSA) (Srinivasan et al., 1998), as implemented in the AMBER 9 suite, was applied to the theoretical structures to quantify the energy differences between side chain rotamer conformations. Representative structures for each trajectory were selected automatically by clustering the structures in the ensemble into conformationally related subfamilies using the program NMRClust (Kelley et al., 1996).

2.3. Quantum mechanical calculations

Full geometry optimizations of the Ace-$(Ala)_5$-Ser-$(Ala)_3$-NHMe α-helix were performed at the B3LYP/6–31G level of theory. The side chain of Ser was built in the *g*+ and *g*− (either with its Hγ atom pointing towards the $i-3$ or the $i-4$ carbonyl) conformations. Electrostatic potentials and atomic point charges were calculated at the B3LYP/6–31G* level of theory. The effect of the surrounding medium was included using the polarizable continuum model (PCM) with cyclohexane as a solvent ($\varepsilon = 2.0165$) (Tomasi et al., 2005), which mimics the membrane environment (Allen, 2007). Quantum chemical calculations were performed with the GAUSSIAN-03 package (Frisch et al., 2004).

2.4. Quantification of transmembrane helices structural distortions

2.4.1. Dihedral backbone torsion angles

The φ and ψ dihedral backbone torsion angles at position *i*, containing either Ala (used as control), Ser or Thr in the helix stretches extracted from the experimental structures (Ala^{PDB}, $Ser^{PDB}g-$, $Ser^{PDB}g+$, $Ser^{PDB}t$, $Thr^{PDB}g-$, $Thr^{PDB}g+$, $Thr^{PDB}t$) and from the theoretical structures obtained by MD simulations (Ala^{MD}, $Ser^{MD}g-$, $Ser^{MD}i-3$, $Ser^{MD}i-4$, $Ser^{MD}g+$, $Thr^{MD}g-$, and $Thr^{MD}g+$) were calculated for statistical analysis. We have previously shown that Ser or Thr side chains do not influence dihedral angles at other positions in the helix (Ballesteros et al., 2000).

2.4.2. Helix bend

Bend angles reported in Table 2 were calculated (see Supplementary Material for details) as the angle between the axes computed as the least square lines through the backbone atoms of the residues preceding and following the motif that induces the distortion in the helix (Chou et al., 1984). In addition, local bend angles of the M2 helix of *Escherichia coli* aquaporin Z (PDB ID: 1RC2) and TM5 of the human β_2-adrenergic receptor (PDB ID: 2RH1) were calculated for each set of four contiguous residues, using the program Helanal (Bansal et al., 2000).

2.4.3. Helix twist

Unit twist angle (Bansal et al., 2000) is a particularly useful measure of helix uniformity at a local level. This parameter is calculated for sets of four consecutive Cα atoms, and it is interpreted as follows: an ideal α-helix, with approximately 3.6 residues per turn, has a twist angle of approximately 100° (360°/3.6); a closed helix segment, with <3.6 residues per turn, possesses a twist >100°; whereas an open helix segment, with >3.6 residues per turn, possesses a twist <100°.

Table 2
Means and standard deviations of the backbone φ and ψ dihedral angles of Ala, Ser and Thr residues, in degrees, calculated from the PDB structures (Ala^{PDB}, $Thr^{PDB}g-$, $Ser^{PDB}g-$, $Thr^{PDB}g+$, $Ser^{PDB}g+$, $Thr^{PDB}t$, $Ser^{PDB}t$) and from the MD simulations (Ala^{MD}, $Thr^{MD}g-$, $Ser^{MD}g-$, $Thr^{MD}g+$, $Ser^{MD}g+$, $Ser^{MD}i-3$, $Ser^{MD}i-4$), in which case the bend angle is also shown. *N* is the number of structures in each category. Statistically significant differences relative to the controls Ala^{PDB} and Ala^{MD} are shown in bold ($p < 0.05$).

	Control	*g*−		*g*+		*trans*	
	Ala^{PDB}	$Ser^{PDB}g-$	$Thr^{PDB}g-$	$Ser^{PDB}g+$	$Thr^{PDB}g+$	$Ser^{PDB}t$	$Thr^{PDB}t$
PDB structures							
N	348	27	22	57	118	20	4
φ	−61.2/12.1	***−65.7/9.5***	***−66.5/5.5***	−63.6/9.4	−62.1/11.1	−64.3/10.7	***−75.0/8.9***
ψ	−43.9/10.8	***−32.0/10.1***	***−34.3/11.5***	−42.5/12.0	−45.1/15.7	−40.3/9.4	***−31.5/6.7***
	Control	*g*−				*g*+	
	Ala^{MD}	$Ser^{MD}g-$	$Thr^{MD}g-$	$Ser^{MD}i-3$	$Ser^{MD}i-4$	$Ser^{MD}g+$	$Thr^{MD}g+$
MD simulations							
N	100	100	100	100	100	100	100
φ	−61.2/8.3	***−64.1/7.7***	***−66.2/8.6***	−62.9/7.4	***−66.1/9.7***	−62.3/8.5	−63.6/9.4
ψ	−44.1/8.5	***−39.1/8.4***	***−38.5/9.9***	***−39.6/7.1***	***−39.8/8.6***	−44.7/8.2	−43.8/8.0
Bend	10.5/5.4	***12.5/4.5***	***12.0/5.5***	11.4/5.2	***12.2/4.6***	10.8/5.1	10.4/4.8

2.5. Statistical analysis

One-way analysis of variance for independent samples plus a posteriori two-sided Dunnett's T test was employed to compare the φ and ψ torsion angles, bend angle, and twist angles of the Ser and Thr residues with the control (Ala).

3. Results and discussion

3.1. Influence of Ser and Thr side chain conformation in the structure of the helix backbone

Table 2 summarizes the mean and standard deviation of the backbone φ and ψ dihedral angles of Ser and Thr residues in their possible rotamer conformations and of Ala (control) calculated from the experimental structures extracted from the Protein Data Bank (i.e. Ala^{PDB}, $Ser^{PDB}g-$, $Thr^{PDB}g-$, $Ser^{PDB}g+$, $Thr^{PDB}g+$, $Ser^{PDB}t$, and $Thr^{PDB}t$). We have previously shown that there is a clear influence of the environment on the main chain conformation (φ and ψ dihedral angles) of α-helices (Olivella et al., 2002). Thus, in contrast to our previous analysis (Ballesteros et al., 2000), only helix stretches with Ala/Ser/Thr exposed to the membrane were kept for analysis, in order to avoid interfering effects of other residues of the protein core (see Section 2). The results show that there are no statistical differences between the backbone φ and ψ dihedral angles of Ser and Thr in the $g+$ conformation ($Ser^{PDB}g+$, $Thr^{PDB}g+$) and the control Ala (Ala^{PDB}). On the other hand, while the t conformation of Ser ($Ser^{PDB}t$) does not modify φ and ψ relative to the control Ala^{PDB}, Thr in t ($Thr^{PDB}t$) results in a statistically significant decrease in φ and increase in ψ. The steric clash between the methyl group of Thr and the backbone carbonyl at the $i-3$ position (McGregor et al., 1987), which is absent in Ser, is responsible for this distortion in the backbone structure. Finally, the $g-$ conformation of both Ser and Thr is related to a statistically significant change in both φ and ψ relative to the control. Specifically, $Ser^{PDB}g-$ decreases φ by $-4.5°$ and increases ψ by 11.9°, whereas $Thr^{PDB}g-$ decreases φ by $-5.3°$ and increases ψ by 9.6°. Thus, the enlarged database of membrane proteins of the present study, which only accounts for side chains exposed to the lipid environment, confirms and reinforces the statistical significance of our previous findings (Ballesteros et al., 2000).

Table 2 also shows the backbone φ and ψ dihedral angles calculated from the structures obtained in the MD trajectories of the model systems (i.e. Ala^{MD}, $Ser^{MD}g-$, $Thr^{MD}g-$, $Ser^{MD}g+$, $Thr^{MD}g+$). First of all, it is worth to notice the remarkable coincidence between the φ and ψ angles obtained in the analysis of the structure of Ala residues in membrane proteins (Ala^{PDB}) and in computer simulations (Ala^{MD}) (φ, $-61.2°$ vs. $-61.2°$; ψ, $-43.9°$ vs. $-44.1°$). Notably, the effect of the $g-$ conformation of Ser and Thr in the MD simulations is the same, in both magnitude and direction, as the observed in the protein survey analysis. $Ser^{MD}g-$ decreases φ by $-2.9°$ and increases ψ by 5.0°, whereas $Thr^{MD}g-$ decreases φ by $-5.0°$ and increases ψ by 5.6°, relative to the control (Ala^{MD}). Moreover, there are no statistical differences between both Ser and Thr in $g+$ ($Ser^{MD}g+$, $Thr^{MD}g+$) relative to the control (Ala^{MD}), as found in the experimental structures. Thus, the explicit methane molecules in our MD simulations that mimic the hydrophobic environment of the cell membrane core reproduce the structural characteristics of TMs.

During our MD simulations the side chain of both Ser and Thr residues in the $g+$ conformation always form a hydrogen bond interaction with the backbone carbonyl oxygen at position $i-4$ (Fig. 1A and D). On the other hand, when the side chain of these residues are in the $g-$ conformation, Ser can form a hydrogen bond with either the carbonyl oxygen at position $i-4$ (66% of the structures, Fig. 1B) or $i-3$ (34%, Fig. 1C), whereas Thr is primarily hydrogen bonding the carbonyl oxygen at position $i-4$ (95%, Fig. 1E). The overwhelming preference of Thr, relative to Ser, in $g-$ for the interaction with the $i-4$ carbonyl is due to the steric restriction of the additional methyl group of Thr in the $i-3$ hydrogen bond interaction with the carbonyl in the previous turn of the helix (Deupi et al., 2004). The absence of the Hγ atom of Ser and Thr in the crystal structures does not allow a straightforward identification of which carbonyl oxygen the OγH side chain preferentially hydrogen bonds to, since the Oγ atom is located roughly midway the carbonyl oxygen at positions $i-3$ and $i-4$ (compare Fig. 1B and C). Thus, the influence of the hydrogen bond interaction to the O_{i-3} or the O_{i-4} carbonyl oxygen on the backbone φ and ψ dihedral angles can only be studied unambiguously from the structures obtained in the MD simulations of Ser in the $g-$ conformation, which, as we have shown before, accurately reproduce the structural characteristics of TMs. Table 2 shows the backbone φ and ψ dihedral angles calculated from the MD trajectories in which either the $O\gamma H\cdots O_{i-3}$ or $O\gamma H\cdots O_{i-4}$ hydrogen bond was restrained (see Section 2). The $O\gamma H\cdots O_{i-4}$ ($Ser^{MD}i-4$) hydrogen bond has an effect in φ and ψ similar to the $Ser^{MD}g-$ simulation: φ decreases $-4.9°$ and ψ increases 4.3°, relative to the control (Ala^{MD}). In contrast, the $O\gamma H\cdots O_{i-3}$ ($Ser^{MD}i-3$) hydrogen bond does not significantly modify φ relative to the control, while ψ increases 4.5°. Thus, we hypothesize that the most abundant and more stable (see below) $O\gamma H\cdots O_{i-4}$ hydrogen bond of Ser in the $g-$ conformation is responsible for the local structural changes induced in the backbone conformation of the helix.

In summary, these results clearly indicate that the $g-$ conformation of Ser and Thr is responsible of highly localized distortions in the α-helix.

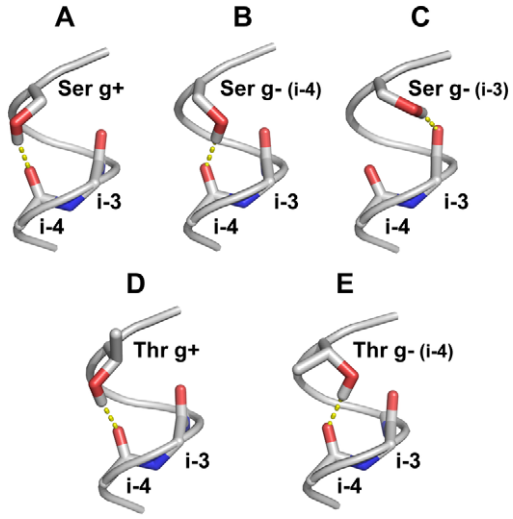

Fig. 1. Detailed view of the hydrogen bond pattern of Ser in $g+$ (A) and $g-$ (B and C), and Thr in $g+$(D) and $g-$ (E) conformations. These structures were selected from the MD trajectories using the program NMRclust and their geometry was optimized by energy minimization using AMBER 9 (see Section 2). The side chain of Ser in $g-$ can form a hydrogen bond with either the carbonyl oxygen at position $i-4$ (B) or $i-3$ (C), whereas Thr is primarily hydrogen bonding the carbonyl oxygen at position $i-4$ (E).

3.2. Energy differences between side chain rotamer conformations

The generation of an ensemble of structures of TMs by MD simulations allows us to perform a statistical analysis of the energy differences between the rotamer conformations and hydrogen bond interactions of Ser and Thr residues using the MM-PBSA method (Srinivasan et al., 1998). Our calculations show that the

g+ rotamer is the lowest energy conformation of Ser, the g− conformation is 1.7 kcal/mol higher if the side chain is hydrogen bonding the backbone carbonyl at the $i-4$ position and 4.6 kcal/mol higher if interacting with the carbonyl at the $i-3$ position. Thr follows similar trends in its two allowed conformations: the g+ rotamer is the lowest energy conformation, and the g− rotamer is 1.1 kcal/mol higher. These results are in qualitative agreement with the rotamer populations observed in the database of membrane proteins, where the g+ conformation of both Ser and Thr is more common than the g−.

3.3. The g− rotamer conformation induces a modest increase of the bend angle and a local opening of the helix

Table 2 shows the mean and standard deviation of the bend angle (see Section 2) calculated from the structures obtained during the MD trajectories. The bend angle measured for an ideal polyalanine α-helix (Ala^{MD}) is 10.5°. This value is a measure of the inherent dynamic flexibility of the helix, which results in this non-directional bend. Notably, Ser and Thr in the g− conformation induce and/or stabilize a modest, albeit statistically significant, increase of the bend angle (12.5° for Ser and 12.0° for Thr, Table 2). As expected, this increase in the bend angle is not detected in the g+ conformation (Table 2). This method to quantify the bend angle cannot be applied to the shorter structures extracted from the PDB, as the calculation of helix axis on very short helices is extremely sensitive to small structural variations (results not shown).

Local structural changes are best described by helix twists (see Section 2). Fig. 2 shows the pattern of the unit twist angles along the helices of the MD-generated ensemble, from turns ($i-10$, $i-7$) to ($i+2$, $i+4$), in which position i was assigned to Ser or Thr. Notably, both Ser and Thr in g−, with the side chain hydrogen bonding the carbonyl at position $i-4$, open the helix at the turns between residues i and $i-5$. This effect is not present in Ser/Thr in g+, or Ser in g− hydrogen bonding the $i-3$ carbonyl.

3.4. Molecular mechanism of helix distortion by the g− conformation

In order to understand the fundamental basis of the influence of the g− conformation on the local structure of α-helices, we performed quantum mechanical calculations on the Ace-$(Ala)_5$-Ser-$(Ala)_3$-NHMe model peptide. Ser was chosen instead of Thr because its side chain in g− can form hydrogen bond interactions with both the carbonyls at positions $i-3$ ($O\gamma H\cdots O_{i-3}$) and $i-4$ ($O\gamma H\cdots O_{i-4}$). Fig. 3 shows the optimized geometries as well as the calculated electrostatic potential surfaces (see Section 2), which show that the negatively charged area created by the OγH side chain of Ser points to different positions in space depending on its rotamer conformation. In the g+ conformation (Fig. 3a), the OγH group points away from the helix, whereas in the g− conformation it is located roughly between the backbone carbonyls of the residues at positions $i-3$ and $i-4$ (Fig. 3b and c). Therefore, hydrogen bonding of OγH to one of these carbonyls leads to an unfavorable interaction with the other one, due to the electrostatic repulsion between the oxygen atoms. However, the $O\gamma\cdots O_{i-3}$ distance (3.3 Å) in the $O\gamma H\cdots O_{i-4}$ hydrogen bond (Fig. 3c) is noticeably shorter than the $O\gamma\cdots O_{i-4}$ distance (4.0 Å) in the $O\gamma H\cdots O_{i-3}$ hydrogen bond (Fig. 3b). Furthermore, the $O\gamma H\cdots O_{i-4}$ hydrogen bond (Fig. 3c) orients the Ser side chain such that the negatively charged areas corresponding to Oγ and O_{i-3} point directly towards each other (Fig. 3c, inset). Thus, the shorter $O\gamma\cdots O{=}C$ distance in the $O\gamma H\cdots O_{i-4}$ hydrogen bond results in a stronger repulsive interaction. We hypothesize that the helix distortion observed in the g− conformation is due to this repulsion. The helix opens up and bends at the turn preceding Ser/Thr in order to minimize the repulsive force between the negatively charged oxygens.

4. Conclusions

Ser and Thr are the most prevalent polar residues in TMs, each constituting 5% of the residues (Senes et al., 2000). These amino

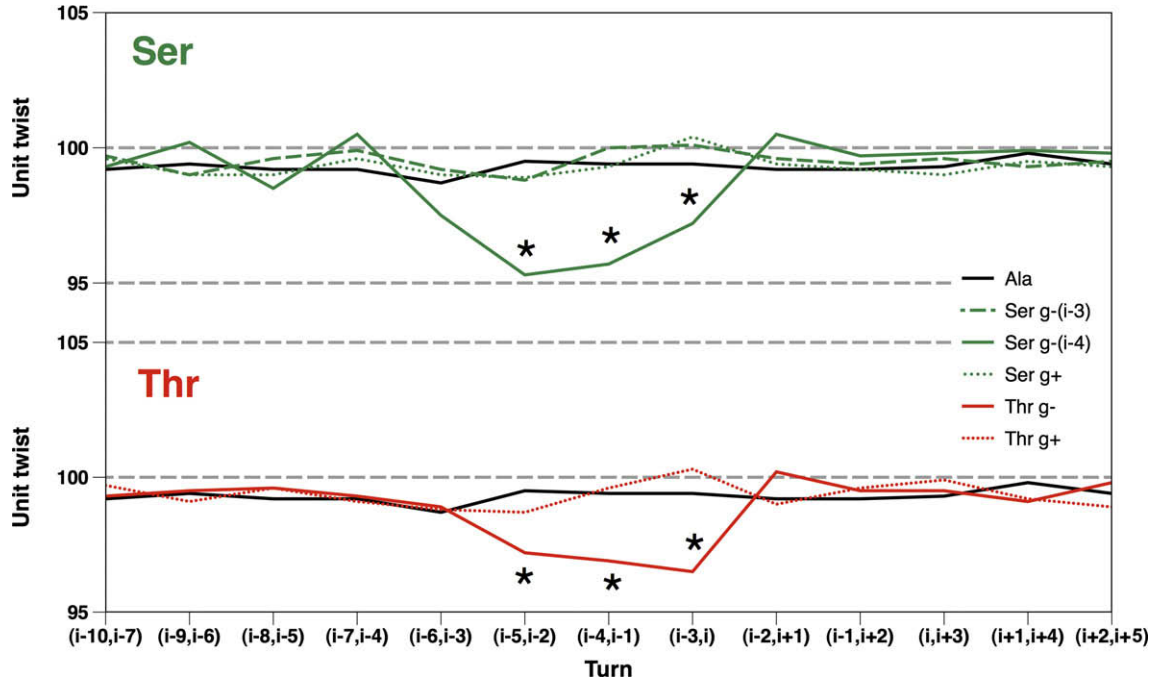

Fig. 2. Evolution of unit twist angles along the α-helices obtained during the MD simulations, from turns ($i-10$, $i-7$) to ($i+2$, $i+4$), in which position i was assigned to Ser or Thr. The color and style codes are: Ala (control, solid black lines), Ser (green lines), Thr (red lines), g+ conformation (dotted lines), and g− conformation with the side chain hydrogen bonding the carbonyl at position $i-3$ (dashed lines) and $i-4$ (solid lines). Statistically significant differences relative to the control are shown by $^*p < 0.05$. Clearly, Ser and Thr residues in the g− conformation, hydrogen bonding the carbonyl at the $i-4$ position, induce a local opening in the preceding turn of the helix.

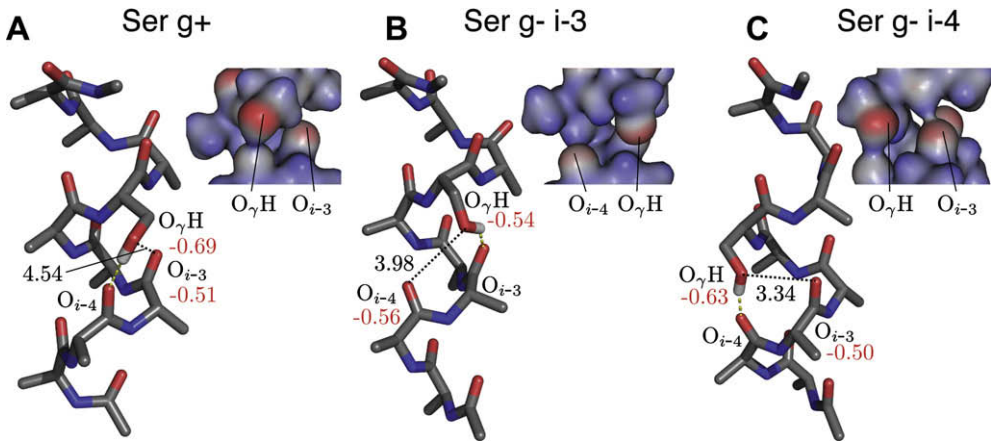

Fig. 3. *Ab initio* geometry optimization of the Ace-(Ala)5-Ser-(Ala)3-NHMe model peptide and calculated electrostatic potential surfaces. The side chain of Ser is in the *g*+ conformation (a) and *g*− conformation with the side chain hydrogen bonding either the carbonyl at position $i-3$ (b) or $i-4$ (c).

acids, unlike other polar or charged residues, do not destabilize TMs (Monne et al., 1999), as their hydrogen bonding potential can be satisfied by interacting with the carbonyl oxygen in the preceding turn of the same helix (Gray and Matthews, 1984) (Fig. 1). To assess the influence of this side chain-backbone hydrogen bond interaction in the structure of TMs, we have used two complementary approaches: analysis of TMs in crystal structures of membrane proteins, and MD simulations on TMs embedded in a non-polar solvent. Both analyses show (Table 2) that Ser and Thr in the *g*+ conformation do not modify the conformation of TMs. In contrast, Ser and Thr in the *g*− conformation, when hydrogen bonding the carbonyl at position $i-4$, induce and/or stabilize a structural change in the helix backbone (Table 2). Quantum mechanical calculations reveal that this effect can be attributed to the repulsion between the negatively charged areas created by the OγH side chain and the backbone carbonyl oxygen at position $i-3$ (Fig. 3).

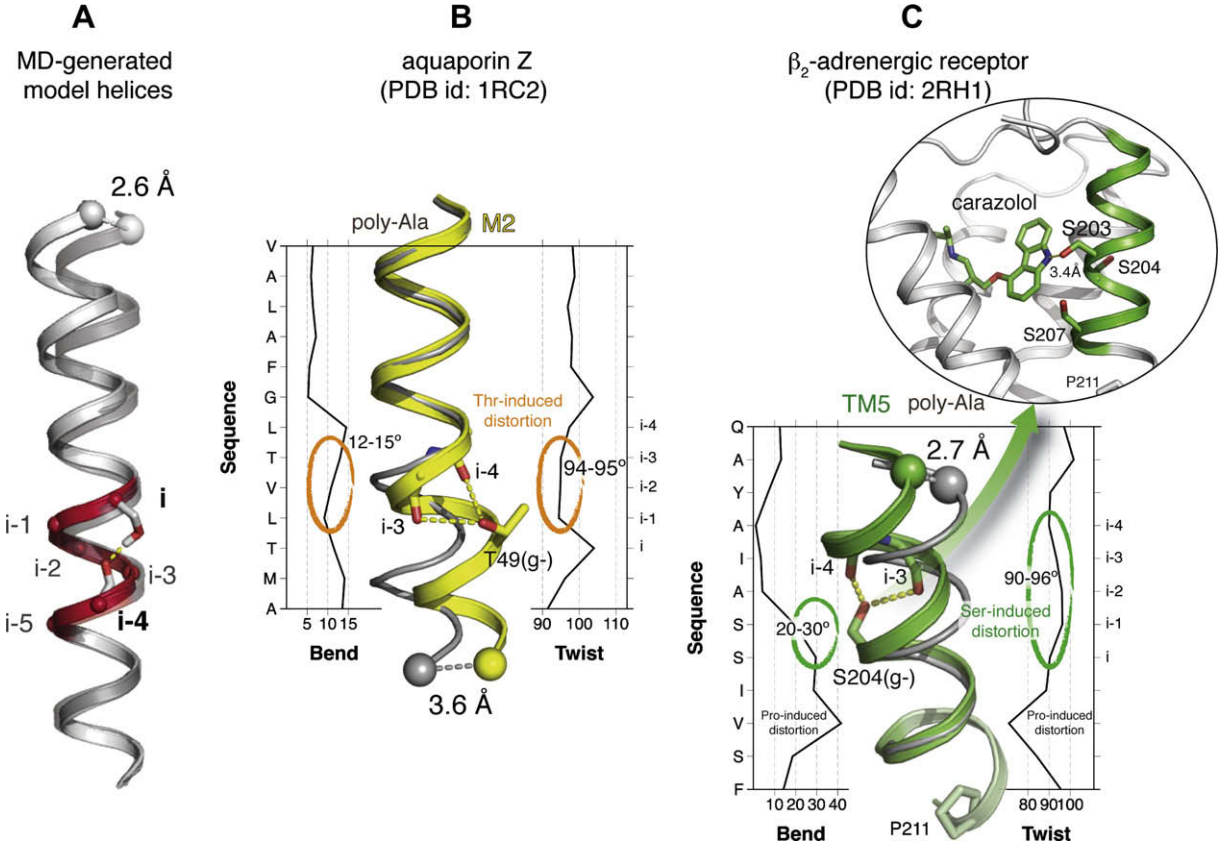

Fig. 4. (A) Representative structures of $Ser^{MD}i-4$ (solid ribbon) and $Ser^{MD}g+$ (translucent ribbon) model peptides, as obtained in the MD trajectories (see legend of Fig. 1 for details), superimposed in their N-terminal sides. The local opening of the helix (see Fig. 2) induced by the *g*− conformation of Ser/Thr, between positions *i* and $i-5$, are colored in red. This local distortion in the middle of the helix can induce a displacement of the residues located three turns away of up to 2.6 Å. (B) The M2 helix (in yellow) of the *E. coli* aquaporin Z (PDB ID: 1RC2) superimposed (residues 38–45) to an ideal poly-Ala helix (in gray). (C) TM5 (in green) of the human β_2-adrenergic receptor (PDB ID: 2RH1) superimposed (residue 205–208) to an ideal poly-Ala helix (in gray). The distortion/bending of the helix facilitates the interaction between Ser203 and the inverse agonist carazolol (top inset). The distortion in the helix caused by Thr49 (B) or Ser204 (C) in the *g*− conformation is monitored by the local bend (left plot) and twist (right plot) angles as calculated with the HelAnal program (Bansal et al., 2000) (see Section 2).

This repulsion is not present in the *g*+ conformation since the negative area of OγH is pointing outside the helix segment. We have estimated the energy difference between these *g*− and *g*+ conformations in 1.1–1.7 kcal/mol. Thus, thermal energy or ligand binding can easily provide this energy, which can be translated into structural changes in the backbone.

In order to quantify both local and global structural changes induced by the *g*− conformation of Ser and Thr we calculated helix bends and twists of the TMs (see Section 2). Analysis of these parameters in the MD-generated ensemble of structures show that, in contrast to *g*+, the *g*− conformation of Ser and Thr induces and/or stabilizes a modest, albeit statistically significant, increase of the bend angle (Table 2) and a local opening of the helix at the turn preceding Ser/Thr (Fig. 2), in order to minimize the repulsion between the negatively charged oxygens (Fig. 3). These effects can be important for the local helix structure (i.e. changing the position of nearby residues) or can be translated/amplified through the α-helix. The magnitude of this effect can be estimated from the models depicted in Fig. 4A, in which representative structures (see Section 2) from the MD trajectories of Ser in *g*− (solid ribbon) and in *g*+(translucent ribbon) are superimposed in their N-terminal sides. The local opening of the helix (Fig. 2) induced by the *g*− conformation between positions i and $i-5$ is colored in red. Notably, the distance between the α-carbon positions of the *g*− and *g*+ helices is 2.6 Å for an amino acid located three turns away. Thus, the modest structural distortion in the middle of the helix results in a significant displacement of the residues located at the other side of the helix. The crystal structures of the M2 helix of *E. coli* aquaporin Z (PDB ID: 1RC2) and TM5 of the human β_2-adrenergic receptor (PDB ID: 2RH1) can be used to illustrate these Ser/Thr-induced structural distortions. Fig. 4B shows the M2 helix of aquaporin (in yellow) superimposed to an ideal poly-Ala helix (in gray). The side chain of Thr49 in *g*− hydrogen bonds the backbone carbonyl of Leu45 at position $i-4$, stabilizing a distortion of the helix that relocates the intracellular part of the helix by 3.6 Å. Thus, M2 of aquaporin displays, in the previous turn of Thr49, an increase of local bend angles to values in the 12–15° range and a local opening of the helix (unit twist of ∼95°) as shown in Fig. 4B. Similar effects are observed in TM5 of the β_2-adrenergic receptor (Fig. 4C). Ser204 in *g*− hydrogen bonds the backbone carbonyl of Ala200, increasing bend angles to 20–30° and a local opening of the helix (unit twist of ∼90–96°). This bend of TM5 toward the protein core, induced or stabilized by Ser204, results in a tightening of the binding pocket, which is required for productive binding of small-molecule agonists (Rosenbaum et al., 2009; Nygaard et al., 2009).

There are several studies that relate primary sequences to α-helical structures. For instance, α-helical membrane proteins contain numerous non-regular short segments (Riek et al., 2001), and their occurrence and conservation are encoded in short peptidic sequences (Rigoutsos et al., 2003). Our study suggests that individual Ser and Thr residues can form part of these sequences, as it has been extensively shown for individual Pro residues (Cordes et al., 2002). In addition, an extension of our results to other residues would open the possibility of building "side chain-dependent backbone structure libraries", similar to the successful backbone-dependent rotamer libraries for side chains, that would help the efforts to model the conformational states accessible to the protein backbone (Baeten et al., 2008).

In summary, Ser and Thr in helix segments of TM proteins can induce and/or stabilize local structural distortions, which can be relevant to structure prediction, protein and drug design and the study of activation mechanisms for membrane proteins. Thus, identification of conserved Ser and Thr residues in multiple sequence alignment can suggest putative residues that can play a role in protein structure and/or function.

Acknowledgments

This work has been supported by grants from the Ministerio de Educación y Ciencia (Spain) (MEC, SAF2006-04966, SAF2007-67008) and Instituto de Salud Carlos III (RD07/0067/0008). X.D. is supported by MEC through the Ramon y Cajal program.

Appendix A. Supplementary data

Supplementary data associated with this article can be found, in the online version, at doi:10.1016/j.jsb.2009.09.009.

References

Allen, T.W., 2007. Modeling charged protein side chains in lipid membranes. J. Gen. Physiol. 130, 237–240.
Baeten, L., Reumers, J., Tur, V., Stricher, F., Lenaerts, T., Serrano, L., Rousseau, F., Schymkowitz, J., 2008. Reconstruction of protein backbones from the brix collection of canonical protein fragments. PLoS Comput. Biol. 4, e1000083.
Ballesteros, J.A., Deupi, X., Olivella, M., Haaksma, E.E.J., Pardo, L., 2000. Serine and threonine residues bend α-helices in the $\chi_1 = g-$ conformation. Biophys. J. 79, 2754–2760.
Bansal, M., Kumar, S., Velavan, R., 2000. Helanal: a program to characterize helix geometry in proteins. J. Biomol. Struct. Dyn. 17, 811–819.
Berman, H.M., Westbrook, J., Feng, Z., Gilliland, G., Bhat, T.N., Weissig, H., Shindyalov, I.N., Bourne, P.E., 2000. The Protein Data Bank. Nucleic Acids Res. 28, 235–242.
Bowie, J.U., 2005. Solving the membrane protein folding problem. Nature 438, 581–589.
Case, D.A., Darden, T.A., Cheatham III, T.E., Simmerling, C.L., Wang, J., Duke, R.E., Luo, R., Merz, K.M., Pearlman, D.A., Crowley, M., Walker, R.C., Zhang, W., Wang, B., Hayik, S., Roitberg, A., Seabra, G., Wong, K.F., Paesani, F., Wu, X., Brozell, S., Tsui, V., Gohlke, H., Yang, L., Tan, C., Mongan, J., Hornak, V., Cui, G., Beroza, P., Mathews, D.H., Schafmeister, C., Ross, W.S., Kollman, P.A., 2006. AMBER 9. University of California, San Francisco.
Chamberlain, A.K., Bowie, J.U., 2004. Analysis of side-chain rotamers in transmembrane proteins. Biophys. J. 87, 3460–3469.
Chou, K.C., Nemethy, G., Scheraga, H.A., 1984. Energetic approach to the packing of α-helices. 2. General treatment of nonequivalent and nonregular helices. J. Am. Chem. Soc. 106, 3161–3170.
Cordes, F.S., Bright, J.N., Sansom, M.S., 2002. Proline-induced distortions of transmembrane helices. J. Mol. Biol. 323, 951–960.
Dawson, J.P., Weinger, J.S., Engelman, D.M., 2002. Motifs of serine and threonine can drive association of transmembrane helices. J. Mol. Biol. 316, 799–805.
Deupi, X., Olivella, M., Govaerts, C., Ballesteros, J.A., Campillo, M., Pardo, L., 2004. Ser and thr residues modulate the conformation of pro-kinked transmembrane alpha-helices. Biophys. J. 86, 105–115.
Deupi, X., Dolker, N., Lopez-Rodriguez, M., Campillo, M., Ballesteros, J., Pardo, L., 2007. Structural models of class a G protein-coupled receptors as a tool for drug design: insights on transmembrane bundle plasticity. Curr. Top. Med. Chem. 7, 999–1006.
Eilers, M., Patel, A.B., Liu, W., Smith, S.O., 2002. Comparison of helix interactions in membrane and soluble alpha-bundle proteins. Biophys. J. 82, 2720–2736.
Fleishman, S.J., Unger, V.M., Ben-Tal, N., 2006. Transmembrane protein structures without X-rays. Trends Biochem. Sci. 31, 106–113.
Frenkel, D., Smit, B., 1996. Understanding Molecular Simulation. From Algorithms to Applications. Academic Press, San Diego.
Frisch, M.J., Trucks, G.W., Schlegel, H.B., Scuseria, G.E., Robb, M.A., Cheeseman, J.R., Montgomery, J.J.A., Vreven, T., Kudin, K.N., Burant, J.C., Millam, J.M., Iyengar, S.S., Tomasi, J., Barone, V., Mennucci, B., Cossi, M., Scalmani, G., Rega, N., Petersson, G.A., Nakatsuji, H., Hada, M., Ehara, M., Toyota, K., Fukuda, R., Hasegawa, J., Ishida, M., Nakajima, T., Honda, Y., Kitao, O., Nakai, H., Klene, M., Li, X., Knox, J.E., Hratchian, H.P., Cross, J.B., Bakken, V., Adamo, C., Jaramillo, J., Gomperts, R., Stratmann, R.E., Yazyev, O., Austin, A.J., Cammi, R., Pomelli, C., Ochterski, J.W., Ayala, P.Y., Morokuma, K., Voth, G.A., Salvador, P., Dannenberg, J.J., Zakrzewski, V.G., Dapprich, S., Daniels, A.D., Strain, M.C., Farkas, O., Malick, D.K., Rabuck, A.D., Raghavachari, K., Foresman, J.B., Ortiz, J.V., Cui, Q., Baboul, A.G., Clifford, S., Cioslowski, J., Stefanov, B.B., Liu, G., Liashenko, A., Piskorz, P., Komaromi, I., Martin, R.L., Fox, D.J., Keith, T., Laham, M.A.A., Peng, C.Y., Nanayakkara, A., Challacombe, M., Gill, P.M.W., Johnson, B., Chen, W., Wong, M.W., Gonzalez, C., Pople, J.A., 2004. Gaussian 03, Revision d.01.
Govaerts, C., Blanpain, C., Deupi, X., Ballet, S., Ballesteros, J.A., Wodak, S.J., Vassart, G., Pardo, L., Parmentier, M., 2001. The TxP motif in the second transmembrane helix of CCR5: a structural determinant in chemokine-induced activation. J. Biol. Chem. 276, 13217–13225.
Gray, T.M., Matthews, B.W., 1984. Intrahelical hydrogen bonding of serine, threonine and cysteine residues within alpha-helices and its relevance to membrane-bound proteins. J. Mol. Biol. 175, 75–81.
Hornak, V., Abel, R., Okur, A., Strockbine, B., Roitberg, A., Simmerling, C., 2006. Comparison of multiple amber force fields and development of improved protein backbone parameters. Proteins 65, 712–725.

Hubbart, S.J., Thornton, J.M., 1993. NACCESS. Department of Biochemistry and Molecular Biology, University College, London.
Joh, N.H., Min, A., Faham, S., Whitelegge, J.P., Yang, D., Woods, V.L., Bowie, J.U., 2008. Modest stabilization by most hydrogen-bonded side-chain interactions in membrane proteins. Nature 453, 1266–1270.
Jongejan, A., Bruysters, M., Ballesteros, J.A., Haaksma, E., Bakker, R.A., Pardo, L., Leurs, R., 2005. Linking ligand binding to histamine H_1 receptor activation. Nat. Chem. Biol. 1, 98–103.
Kelley, L.A., Gardner, S.P., Sutcliffe, M.J., 1996. An automated approach for clustering an ensemble of NMR-derived protein structures into conformationally-related subfamilies. Protein Eng. 9, 1063–1065.
Lomize, M.A., Lomize, A.L., Pogozheva, I.D., Mosberg, H.I., 2006. OPM: orientations of proteins in membranes database. Bioinformatics 22, 623–625.
Lopez-Rodriguez, M.L., Vicente, B., Deupi, X., Barrondo, S., Olivella, M., Morcillo, M.J., Behamu, B., Ballesteros, J.A., Salles, J., Pardo, L., 2002. Design, synthesis and pharmacological evaluation of 5-hydroxytryptamine(1a) receptor ligands to explore the three-dimensional structure of the receptor. Mol. Pharmacol. 62, 15–21.
McGregor, M.J., Islam, S.A., Sternberg, M.J.E., 1987. Analysis of the relationship between side-chain conformation and secondary structure in globular proteins. J. Mol. Biol. 198, 295–310.
Monne, M., Hermansson, M., von Heijne, G., 1999. A turn propensity scale for transmembrane helices. J. Mol. Biol. 288, 141–145.
Munshi, U.M., Pogozheva, I.D., Menon, K.M., 2003. Highly conserved serine in the third transmembrane helix of the luteinizing hormone/human chorionic gonadotropin receptor regulates receptor activation. Biochemistry 42, 3708–3715.
Nygaard, R., Frimurer, T.M., Holst, B., Rosenkilde, M.M., Schwartz, T.W., 2009. Ligand binding and micro-switches in 7tm receptor structures. Trends Pharmacol. Sci. 30, 249–259.
Olivella, M., Deupi, X., Govaerts, C., Pardo, L., 2002. Influence of the environment in the conformation of alpha-helices studied by protein database search and molecular dynamics simulations. Biophys. J. 82, 3207–3213.
Partridge, A.W., Therien, A.G., Deber, C.M., 2004. Missense mutations in transmembrane domains of proteins: phenotypic propensity of polar residues for human disease. Proteins 54, 648–656.
Pellissier, L., Sallander, J., Campillo, M., Gaven, F., Queffeulou, E., Pillot, M., Dumuis, A., Claeysen, S., Bockaert, J., Pardo, L., 2009. Conformational toggle switches implicated in basal constitutive and agonist-induced activated states of 5-HT_4 receptors. Mol. Pharmacol. 75, 982–990.
Riek, R.P., Rigoutsos, I., Novotny, J., Graham, R.M., 2001. Non-alpha-helical elements modulate polytopic membrane protein architecture. J. Mol. Biol. 306, 349–362.
Rigoutsos, I., Riek, P., Graham, R.M., Novotny, J., 2003. Structural details (kinks and non-alpha conformations) in transmembrane helices are intrahelically determined and can be predicted by sequence pattern descriptors. Nucleic Acids Res. 31, 4625–4631.
Rosenbaum, D.M., Rasmussen, S.G., Kobilka, B.K., 2009. The structure and function of g-protein-coupled receptors. Nature 459, 356–363.
Sansom, M.S.P., Weinstein, H., 2000. Hinges, swivels and switches: the role of prolines in signalling via transmembrane α-helices. Trends Pharmacol. Sci. 21, 445–451.
Senes, A., Gerstein, M., Engelman, D.M., 2000. Statistical analysis of amino acid patterns in transmembrane helices: the GxxxG motif occurs frequently and in association with β-branched residues at neighboring positions. J. Mol. Biol. 296, 921–936.
Smit, M.J., Vischer, H.F., Bakker, R.A., Jongejan, A., Timmerman, H., Pardo, L., Leurs, R., 2007. Pharmacogenomic and structural analysis of constitutive g protein-coupled receptor activity. Annu. Rev. Pharmacol. Toxicol. 47, 53–87.
Srinivasan, J., Cheatham, T.E., Cieplak, P., Kollman, P.A., Case, D.A., 1998. Continuum solvent studies of the stability of DNA, rna, and phosphoramidate – DNA helices. J. Am. Chem. Soc. 120, 9401–9409.
Tomasi, J., Mennucci, B., Cammi, R., 2005. Quantum mechanical continuum solvation models. Chem. Rev. 105, 2999–3093.
Tusnady, G.E., Dosztanyi, Z., Simon, I., 2005. PDM_TM: selection and membrane localization of transmembrane proteins in the protein data bank. Nucleic Acids Res. 33, D275–D278.
Yohannan, S., Faham, S., Yang, D., Whitelegge, J.P., Bowie, J.U., 2004. The evolution of transmembrane helix kinks and the structural diversity of G protein-coupled receptors. Proc. Natl. Acad. Sci. USA 101, 959–963.